Progress in Natural Science: Materials International 2013;23(1):51–54

Chinese Materials Research Society

Progress in Natural Science: Materials International

www.elsevier.com/locate/pnsmi
www.sciencedirect.com

ORIGINAL RESEARCH

Facile cathodic electrosynthesis and characterization of iron oxide nano-particles

Taher Yousefi[a,*], Reza Davarkhah[a], Ahmad Nozad Golikand[b], Mohammad Hossein Mashhadizadeh[c], Ahmad Abhari[a]

[a]*NFCRS, Nuclear Science and Technology Research Institute, P.O. Box 11365/8486, Tehran, Iran*
[b]*Materials Research School, NSTRI, P.O. Box: 14395-836 Tehran, Iran*
[c]*Department of Chemistry, Tarbiat Moallem University, P.O. Box: 31979-37551 Tehran, Iran*

Received 24 July 2012; accepted 27 October 2012
Available online 26 February 2013

KEYWORDS

Iron Oxide;
Electrochemical Deposition;
Nano Oxides;
Nanostructures;
Characterization

Abstract Fe_2O_3 nano-particles have been synthesized by simple cathodic electrodeposition from the low-temperature nitrate bath. The morphology and crystal structure of the obtained oxide powder were analyzed by means of scanning and transmission microscopy (SEM and TEM), X-ray diffraction (XRD) and Fourier transform infrared (FTIR) spectroscopy. Thermal behavior and phase transformation during the heat treatment of as-deposited sample were investigated by differential scanning calorimetry (DSC) and thermogramimetric analysis (TGA). The results showed that the deposited Fe_2O_3 was composed of the nanoparticles with grain size of approximately 10–60 nm. A serious problem during cathodic electrodeposition of iron oxide was splashing of deposit into electrolyte due to its low adhesion. This problem was tackled by reducing the bath temperature and dielectric constant of solvent.

1. Introduction

Nanostructures are the focus of many researchers because they often exhibit unique properties, which cannot be achieved by their bulk counterparts [1]. The main objective of nanoscale science and technology has been to synthesize nanomaterials with the controlled size and shape, as well as search for new properties that are not realized in microscale morphologies [2]. Among various nanomaterials, nanostructured metal oxides play an important role in physics, chemistry and material science [2]. Magnetic nanoparticles are an important class of nanostructured metal oxides which possess unique magnetic properties [1]. The potential applications of magnetic nanoparticles include ferrofluids for audio speakers [3], surface functionalized probes for biosensors and targeted drug delivery [4], magnetic storage media, powder compacts for power generation, contrasting agents in magnetic resonance imaging and adsorbents for toxic environmental

*Corresponding author. Tel.: +98 9122 863 669.
E-mail address: Taher_yosefy@yahoo.com (T. Yousefi).

Peer review under responsibility of Chinese Materials Research Society.

ELSEVIER Production and hosting by Elsevier

http://dx.doi.org/10.1016/j.pnsc.2013.01.007

pollutants [5]. Maghemite (γ-Fe_2O_3) is a ferromagnetic oxide that has been widely used as a magnetic recording material for tape drives. In addition, maghemite nanoparticles have been utilized as ferrofluid hyperthermia (MFM) in tumor treatment because of good chemical stability and biocompatibility with high heating capacity in the presence of alternating magnetic fields [5]. Obviously, the properties of iron oxide nanocrystallines sensitively depend on their size and shape. Various procedures including wet chemical [6], electrochemical [7], thermal decomposition techniques [8], and chemical oxidation in polymer [9] have been successfully employed for the synthesis of iron oxides nanostructures. Electrodeposition is a promising alternative technique for fabrication of nanoparticles, because it is simple, inexpensive, fast, operates at near room temperature, and is able to control composition, crystallinity, and properties of the deposit by adjusting deposition conditions. Iron oxide films were both cathodically and anodically electrodeposited [10–12]. In the case of anodic formation of iron oxides, the different phases of the iron oxides–oxyhydroxides, thin films were obtained by adjusting deposition potentials and solution composition [10]. Zotti et al. [13] reported the cathodic electrodeposition of amorphous Fe_2O_3 thin films by reduction of Fe (III) perchlorate in oxygenated acetonitrile where ferric ions reduced with dissolved oxygen to form amorphous Fe_2O_3. Amorphous Fe_2O_3 films were later converted to α-Fe_2O_3 (i.e. hematite) films after heat treatment. Cathodic synthesis of iron oxide in aqueous solvent would be limited by splashing of deposit into electrolyte due to low adhesiveness of the deposit. to overcome this problem, addition of some materials as a binder to electrolyte has been reported [14], however the use of the organic macromolecules as a binder has some limitation such as non-solubility of them in aqueous media and their effect on morphology and structure of products[14]. In the present work we used the cathodic depostion method for synthesis of iron oxide without the use of a binder in methanol–water solvent at low reaction temperature of 8 °C.

2. Experimental

2.1. Preparation of Fe_2O_3

Iron oxide precursor was deposited directly on both sides of the stainless steel cathode (316 L, $20 \times 20 \times 0.5\ mm^2$) under a galvanostatic mode at a cathode current density of 1 mA cm^{-2}. The electrodeposition bath was $Fe(NO_3)_3 \cdot 4\ H_2O$ (0.005 M, Merck) aqueous solution which was fixed at 8 °C. After electrodeposition, the deposited film was rinsed several times in deionized water and dried at room temperature for 48 h. Thereafter, the as-deposited sample was scraped from the steel electrode and subjected to further analysis. Thermal annealing was conducted in air between the room temperature and 200 °C at a heating rate of 10 °C min^{-1}.

2.2. Characterization

The obtained products (thermal annealed) were characterized by X-ray diffraction (XRD, Phillips, PW-1800), scanning electron microscopy (LEO 1455VP) and transmission electron microscopy (TEM, Phillips EM 2085). Fourier transform infrared (FT-IR) spectroscopy of sample was recorded with a KBr pellet on a VECTOR-22 (Bruker) spectrometer ranging from 400 to 4000 cm^{-1}.

3. Result and discussions

3.1. TGA and DSC

Fig. 1a and b. shows the TGA and DSC data for the deposits prepared from the 5 mM $Fe(NO_3)_3$ solutions. As shown in the Fig. 1a, the sample showed a total weight loss of 20 wt% in the temperature range up to 700 °C with most of the weight loss occurring below 200 °C. No weight change was observed in the range of 400–700 °C. The weight loss in this region can be attributed to the liberation of the adsorbed water. In the case of low temperature synthesis due to low kinetics of reactions and low rate of gas bubbling on the surface of electrode the insertion of water molecules into the deposit was high and thus the adsorbed water was high compared to samples synthesized at higher temperature. Therefore as shown from TGA curve the weight loss in our sample is higher than that from those of literature [14].

The corresponding DSC data showed that a broad endothermic peak was around 90 °C (Fig. 1b). DSC data showed two exotherms to be at~300 °C and at~400 °C. The first observed exothermic peak is associated with transformation of FeOOH to γ-Fe_2O_3, and the next sharp exothermic peak at 400 °C is related to recrystallization of to γ-Fe_2O_3 to α-Fe_2O_3[15,16].

3.2. XRD and FTIR

The XRD pattern of the calcined sample at 200 °C is shown in Fig. 2a. All diffraction peaks can be indexed as γ-Fe_2O_3

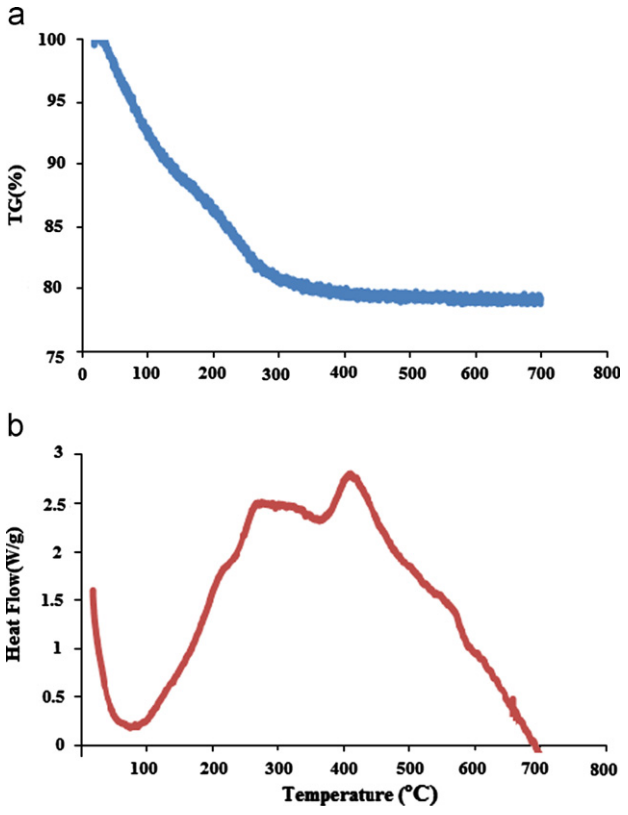

Fig. 1 Thermogravimetric analyses: (a) TGA, (b) DSC of as-prepared sample.

(JCPDS file 39–1346). On the other hand, the peaks at 33 and 63° can be easily indexed to α-Fe_2O_3. We believe that this is an indication that both gamma and alpha phases are present in these samples prepared at low temperature, the amount of the gamma phase is probably small and hence the lower peaks are not visible. γ-Fe_2O_3 has cubic symmetry structure with the space group of P4332 (no. 212). The basic structure of γ-Fe_2O_3 is closely related to the inverse spinel Fe_3O_4, but differs from the latter by the presence of vacancies distributed on the cation lattice. The structure of α-Fe_2O_3, is isostructural with corundrum, α-Al_2O_3. The space group is R3c (rhombohedral symmetry) and the lattice parameters given in the hexagonal cell, are: $a=b=5.0346$ Å and $c=13.752$ Å. Fig. 2b shows the FTIR spectra of calcined sample within the wavelength range of 400–4000 cm^{-1}. The peak at 3450 cm^{-1} indicates the presence of hydroxide group [17]. The peaks at 1658 and 1063 cm^{-1} may be attributed to O–H bending vibrations combined with Fe atoms. The peaks at 605 and 465 cm^{-1} correspond to the metal–oxygen (Fe–O) vibrational modes [17]. The result indicates the presence of Fe–O bonds, and –OH groups for Fe_2O_3 thin films. Thus the formation of Fe_2O_3 compound is confirmed.

3.3. SEM and TEM

SEM and TEM analyses provided the information on the size and shape of particles. Fig. 3a–d show the SEM and TEM images of the sample, which indicate that the sample only consisted of the nano-scale crystallites with fairly uniform size distributions of 10–60 nm. The particles with good crystalline faces and crystallinity state are very well-defined and relatively dispersed.

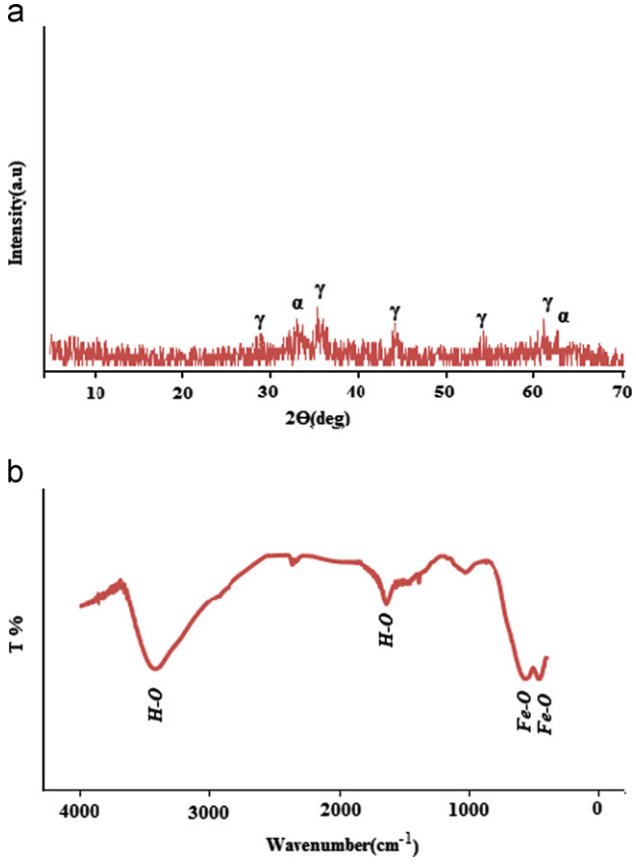

Fig. 2 (a) FTIR spectra and (b) XRD patterns of the sample.

3.4. Electro-deposition mechanism:

Cathodic deposition of oxide/hydroxide is based on the generation of OH^- ions at the working electrode[18–24]. In nitrate solution, the following electrochemical reactions:

$$NO_3^- + H_2O + 2e \rightarrow NO_2^- + 2OH^- \quad (1)$$

$$NO_3^- + 7H_2O + 8e \rightarrow NH_4^+ + 10OH^- \quad (2)$$

$$O_2 + 2H_2O + 4e \rightarrow 4OH^- \quad (3)$$

$$2H_2O + 2e \rightarrow H_2 + 2OH^- \quad (4)$$

may occur at the cathode[18–24]. These reactions cause an increase in local pH on the surface of the cathode and formation of ferric hydroxide9, as shown in Fig. 4. And later ferric hydroxide is converted to form Fe_2O_3. The overall reaction can be shown as

$$6H_2O + 6e \rightarrow 3H_2 + 6OH^- \quad (5)$$

$$2Fe^{3+} + 6OH^- \rightarrow 2Fe(OH)_3$$

$$2Fe(OH)_3 \rightarrow Fe_2O_3 + 3H_2(g)$$

$$2Fe^{3+} + 6OH^- \rightarrow Fe_2O_3 + 3H_2(g)$$

Due to the low concentration of dissolved oxygen and nitrate ions in solution it seems that reaction 4 is dominant in the increase of local pH and hydroxide formation[1]. The loose adhesion of the cathodic iron hydroxide deposits to the cathode surface and their spallation have been reported as common difficulties during electrogeneration of base in aqueous medium. To overcome this problem, we have noticed that the application of lower bath temperature than room temperature can offer important advantages such as control of the kinetic energy of solvents and deposit molecules, in other words at lower temperature the kinetic energy of molecules is low and the adhesion of deposit is firm, thus the spallation can be prevented. Also at low temperature the rate of gas bubbling at electrode surface is reduced and the spallation of deposit into electrolyte would be reduced. Another applied trick for the reduction of the deposit spallation was addition of a solvent with low dielectric constant to the electrolyte, in this way the solvation and separation strength of electrolyte reduced and this caused lower spallation of the deposit. Therefore the certain amount of methanol was added to the electrolyte to reduce the dielectric constant of solvent.

4. Conclusion

The loss adhesion of the cathodic iron oxide deposit to the surface is a common problem in the cathodic electrodeposition of iron oxide. For the first time, low-temperature electro-deposition has been applied in the cathodic electrodeposition of iron oxide. By following this route, nanoparticles of iron oxide were successfully prepared. The sample was characterized by XRD, FTIR, TGA, SEM, and TEM. The

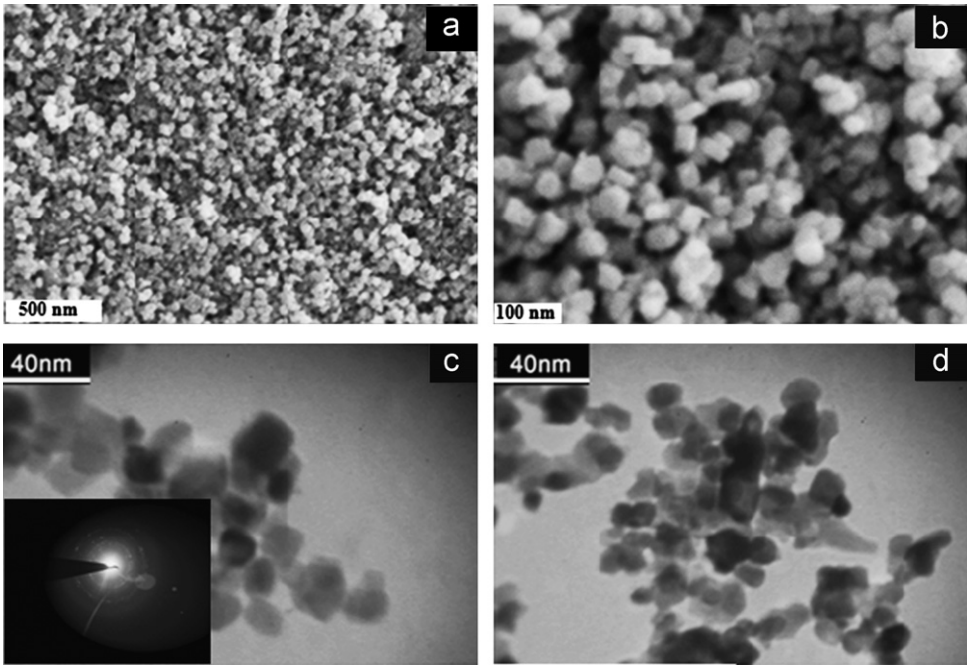

Fig. 3 SEM(a,b) and TEM(c,d, inset SAED pattern) of sample.

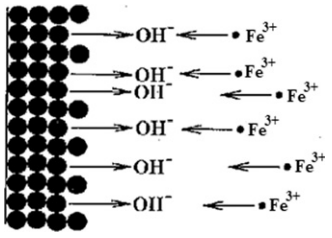

Fig. 4 Cathodic deposition of iron hydroxide/oxide.

average crystalline size distribution of iron oxide was in the range of 10 to 60 nm. The results of this work showed that low-temperature electro-deposition can be recognized as a convenient route in iron oxide cathodic electro-deposition and preparation of its nanostructures.

References

[1] H. Park, P. Ayala, M.A. Deshusses, A. Mulchandani, A. Choi, N.V. Myung, Chemical Engineering Journal 139 (2008) 208–212.
[2] Y. NuLi, R. Zeng, P. Zhang, Z. Guo, H. Liu, Journal of Power Sources 184 (2008) 456–461.
[3] M.M. Miller, G.A. Prinz, S.F. Cheng, S. Bounnak, Applied Physics Letters 81 (2002) 2211–2213.
[4] S. Sun, C.B. Murray, D. Weller, L. Folks, A. Moser, Science 287 (2000) 1989–1992.
[5] J. Hu, G. Chen, I.M.C. Lo, Journal of Environmental Engineering 132 (2006) 709–715.
[6] Z. Jing, S. Wu, S. Zhang, W. Huang, Materials Research Bulletin 39 (2004) 2057.
[7] C. Pascal, J.L. Pascal, F. Favier, M.L.E. Moubtassim, C. Payen, Chemistry of Materials 11 (1999) 141.
[8] J. Cheon, N.J. Kang, S.M. Lee, J.H. Lee, J.H. Yoon, S.J. Oh, Journal of the American Chemical Society 126 (2004) 1950.
[9] R. Ziolo, E.P. Giannelis, B.A. Weinstein, M.P. O'Horo, B.N. Ganguly, V. Mehrotra, Science 257 (1992) 219.
[10] L. Martinez, D. Leinen, F. Martin, M. Gabas, J.R. Ramos-Barrado, E. Quagliata, Journal of the Electrochemical Society 154 (2007) 126–133.
[11] D. Carlier, C. Terrier, C. Arm, J.P. Anserment, Electrochemical and Solid-State Letters 8 (2005) 43–46.
[12] T.A. Sorenson, S.A. Morton, G.D. Waddill, J.A. Switzer, Journal of the American Chemical Society 124 (2002) 7604–7609.
[13] G. Zotti, G. Schiavan, S. Zecchin, Journal of the Electrochemical Society 145 (1998) 385–389.
[14] N. Nagarajan, I. Zhitomirsky, Journal of Applied Electrochemistry 36 (2006) 1399–1405.
[15] J. Cao, I. Zhitomirsky, M. Niewczas, Materials Chemistry and Physics 96 (2006) 289–295.
[16] J.D. Bernal, D.R. Dasgupta, A.L. Mackay, Clay Minerals Bulletin 4 (1959) 15–30.
[17] P.M. Kulal, D.P. Dubal, C.D. Lokhande, V.J. Fulari, Journal of Alloys and Compounds 509 (2011) 2567–2571.
[18] T. Yousefi, A.N. Golikand, M.H. Mashhadizadeh, M. Aghazadeh, Journal of Solid State Chemistry 190 (2012) 202–207.
[19] T. Yousefi, A.N. Golikand, M.H. Mashhadizadeh, M. Aghazadeh, Current Applied Physics 12 (2012) 193–198.
[20] T. Yousefi, A.N. Golikand, M.H. Mashhadizadeha, M. Aghazadeh, Current Applied Physics 12 (2012) 544–549.
[21] T. Yousefi, A.N. Golikand, M.H. Mashhadizadeh, M. Aghazadeh, Journal of the Taiwan Institute of Chemical Engineers 43 (2012) 614–618.
[22] T. Yousefi, M. Aghazadeh, A.N. Golikand, M.H. Mashhadizadeh, Science of Advanced materials 4 (2012) 1–5.
[23] I. Zhitomirsky, Advances in Colloid and Interface Science 97 (2002) 279–317.
[24] G.H.A. Therese, P.V. Kamath, Chemistry of materials 12 (2000) 1195–1204.